Characteristics of an Ultra-Wide-Band Ultra-Wide-Angle Log-Periodic Antenna

Leland M. Cheskis, Marc S. Litz, Neal Tesny, and Lillian Dilks

20010402 027

Army Research Laboratory

Adelphi, MD 20783-1197

Characteristics of an Ultra-Wide-Band Ultra-Wide-Angle Log-Periodic Antenna

Leland M. Cheskis, Marc S. Litz, Neal Tesny, and Lillian Dilks

Sensors and Electron Devices Directorate, ARL

Abstract

A compact ultra-wide-band, ultra-wide-angle log-periodic antenna has been designed by the Mission Research Corporation under a small business innovative research phase II contract with the U.S. Army Research Laboratory (ARL). A proof-of-principle version of the antenna was delivered to ARL. The antenna was evaluated within two days and information returned to the vendor. The calibrations of the antennas included both frequency-domain and time-domain measurements in the High-Power Microwave Anechoic Chamber and the Electromagnetic Research Facility, respectively, and high-voltage-limit characterizations. The appropriate conversion of time-domain and frequency-domain data into gain curves was performed, and the results were discussed. These results are now being applied to the next version of the dual-polarization antenna pair.

Contents

Figures

1. Introduction

The Mission Research Corporation (MRC) designed and built a proof-of-principle ultra-wide-band, ultra-wide-angle (UWB-UWA) log-periodic (LP) antenna for use on the U.S. Army Research Laboratory (ARL) impulse radar. MRC shipped the antenna from its laboratories in Dayton, Ohio, to ARL to characterize it at the ARL Electromagnetic Research Facility (EMRF), which will be referred to as the "cathedral," and in the ARL Anechoic Chamber, which will be referred to as the "chamber." This report describes the time-domain (TD) and frequency-domain (FD) techniques used to evaluate the gain and radiation patterns of the antenna.

The new UWB-UWA LP antenna is an inductively loaded LP antenna (see figure 1(a)). The longest arms of the LP antenna are inductively loaded, which reduces the physical size of the longest arms while maintaining their electrical length. In addition to the size reduction, two cross-polarized LP antennas share the same central support arm but are rotated 90° with respect to each other. The compactness of this system motivates this investigation.

The other antenna, shown in figure 1(b), is a commercial LP antenna. This antenna always served as the receiving antenna in both the cathedral and the chamber, since its properties are well known and reproducible. It remained fixed while the test antenna was rotated.

The relatively small size of the chamber limits its use on the low-frequency end to 200 MHz. To measure the new UWB-UWA LP antenna below this frequency, we used the cathedral, which has no radio frequency (rf) absorber on the walls. Using a 3-ns full-width pulse that includes a frequency content from 50 MHz to 2.5 GHz, we can measure the impulse response of the antenna and calculate its gain. Because the cathedral is large, we can time-gate any reflections that may occur within it. Where measurements provide overlapping results between TD (cathedral) and FD (chamber) techniques, they are compared in this report.

Another objective of this investigation includes determination of the high-voltage limits of the antenna. The LP antenna is not usually considered to be a high-power antenna because of the breakdown that can occur between the many arms of the antenna or in the feed structure. Just how practical is the antenna in a high-voltage, short pulsewidth application? We applied successively larger voltages to the antenna to determine the high-voltage limits.

Figure 1. Antennas
used in experiments:
(a) UWB-UWA LP
antenna and
(b) commercially
available LP antenna.

(a)

(b)

2
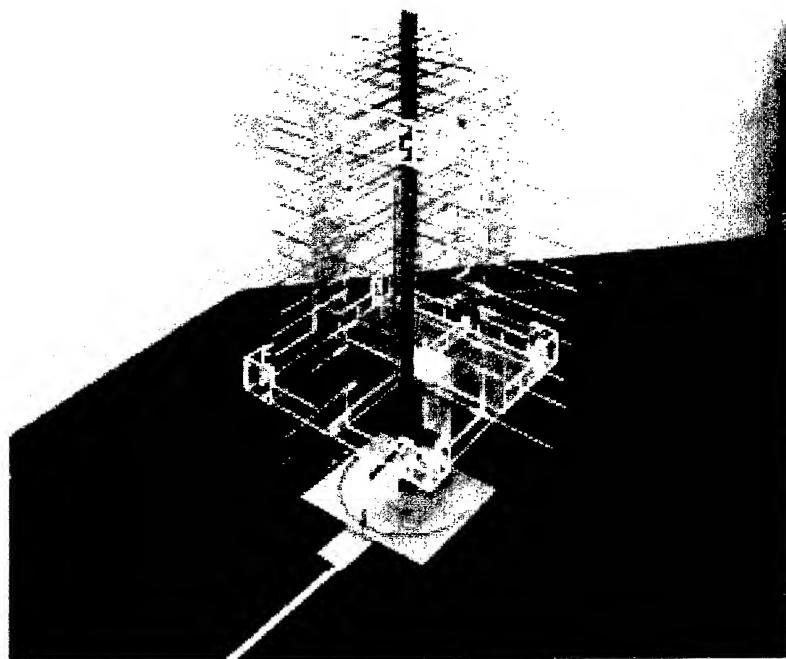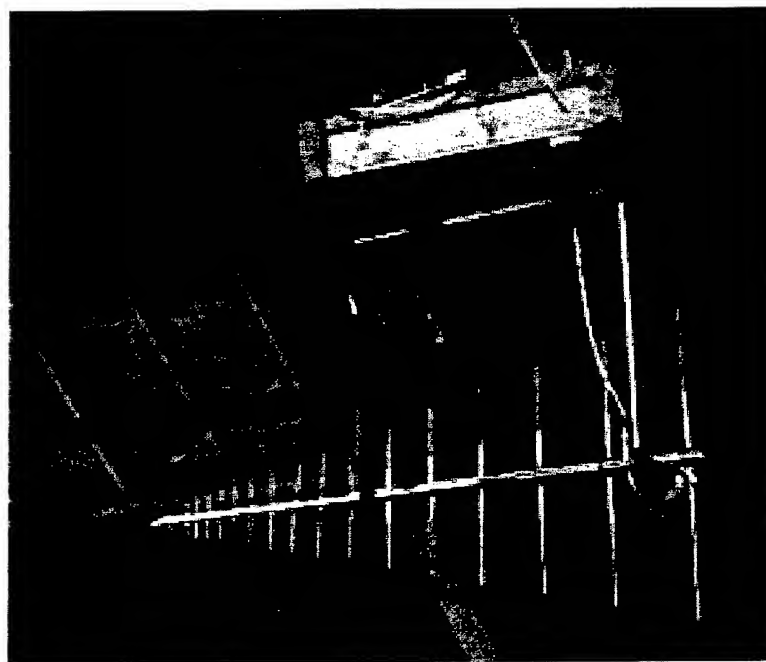
2. Experimental Configuration

Two experimental configurations are described in this section. First, the TD experimental configuration and technique used in the cathedral are described. Then the FD experimental configuration in the chamber and the corresponding instrumentation and techniques are discussed.

2.1 TD Setup

The interior of the EMRF is shown in figure 2. A sandbox appears at the bottom of the figure. The dimensions of the sandbox are $90 \times 60 \times 4$ ft, and the weight of the sand is over 300 tons. Characteristics of the cathedral make it appropriate for testing the UWB-UWA LP antenna. Because the building is constructed of wood, it is transparent to those frequency components below 500 MHz. This construction contributes toward reducing reflections picked up by the receiving antenna. The length of the EMRF (130 ft) means more time can elapse before a reflection off a wall can be detected by the receiving antenna. The antennas were placed at opposite ends of the sandbox, hoisted to 32 ft, and pointed so that they were facing each other.

The UWB-UWA LP antenna was the transmitting antenna in this configuration, and the commercial LP antenna was the receiving antenna. Initially the two antennas directly faced each other. The UWB-UWA antenna, however, was rotated, as will be discussed in the next paragraph. Since the length of the sandbox is 90 ft, the transmitting and receiving antennas were approximately 85 ft apart. This means that the reflected wave, taking the shortest route from the transmitting antenna down to the sandbox and up to the

Figure 2. Inside view of EMRF. Large wooden structure is very useful for TD analysis of impulse signals.

receiving antenna, would lag a direct signal from the transmitting antenna to the receiving antenna by approximately 22 ns. The reflection with the shortest route bounces off the sand midway between the antennas. This midpoint was 45 ft from either end of the sandbox. In other words, this reflection adds to the received signal at the receiving antenna 22 ns after it begins picking up the direct path signal. Reflections came from the metallic garage door behind the receiving antenna, but they arrived after the reflections from the sandbox and are not considered here. The garage door is 35 ft behind the receiving antenna, so any reflections off this door would arrive 70 ns after the direct signal.

An HP 214B pulse generator-fed 11-V trigger pulses with a rise time of less than 10 ns into a Kentec transmitter. The HP 214B operates in a frequency range of 50 to 250 Hz. The 11.5 kV, 2-ns-width output pulses of the Kentec transmitter passed through two attenuators in sequence, attenuating the amplitude by factors of 2 and 3, respectively. This output was then fed to the UWB-UWA antenna, which served as a transmitting antenna. In the cathedral, the UWB-UWA antenna was mounted on an inverted rotating pedestal. It was rotated in 5° increments from –90° to +90° in the horizontal plane.

An antenna consisting of a single dipole can emit a pulse that accurately replicates the shape of the original pulse if the center frequency of the pulse is at or near the resonance of the dipole. If the antenna consists of a sequence of dipoles, as this UWB-UWA LP antenna does, the transmitted pulse is spread out over a much longer time frame than the original pulse, as each dipole radiates near its resonance. As the pulse travels down the center of the antenna, each dipole emits a pulse in turn. In addition, since the receiving antenna at the other end of the sandbox is also LP, the transmitted signal is picked up by a sequence of dipoles and, as a result, is spread out even more.

The electric field has an amplitude of 12.5 V/m at the input of the receiving antenna. Because of the effective length of the antenna, this voltage is multiplied by a factor of 0.2, yielding a voltage signal. This signal passes through a 5× attenuator and a delay line. A signal travels directly to the scope to trigger it. The delay line attenuates the signal by a factor of 2. The resulting signal of 250 mV feeds into a Tektronix 11801 sampling scope.

Each time a signal waveform enters the scope, the scope samples one point from the waveform and stores it. The next time a waveform enters the scope, the scope samples a point that is a specified time further down the waveform. That is, the scope delays sampling a given waveform with respect to the point in time that it sampled the previous waveform, and that delay is a fixed period of time from one waveform to the next. In this manner, 2048 waveforms are sampled in succession to generate one waveform consisting of 2048 points. The effective sampling rate therefore is the inverse of 250 ns/ 2048 points or 8.192 GHz. We take this approach because the technology does not exist to sample 2048 points from a single transient waveform at

that sampling rate. The TD plots used to generate the figures in this report are based on the average of three waveforms, with each waveform consisting of 2048 successive sampled points as described above. The purpose of averaging is to reduce ambient noise. Since the EMRF is a wooden building, it is unable to shield the experiment from the outside world.

As can be seen from the schematic in figure 3, the Tektronix 11801 and the central processing unit (CPU) controller are connected through a general purpose interface bus (GPIB), a fiber-optic line, and a second GPIB. The fiber GPIB is used to eliminate metallic cables in the test area that will contribute to electromagnetic (EM) pickup or radiation that will contribute to the experimental noise background. When the CPU controller receives a signal from the pedestal notifying it that the pedestal has rotated to a new azimuthal setting and the antenna is ready to transmit, it will send a signal through the fiber GPIB to the scope. The scope is alerted to accept signals from the receiving antenna. For each setting of the pedestal, the scope receives a stream of waveforms from the receiving antenna, samples them as discussed in the previous paragraph, and stores the sampled points. When all the waveforms have arrived at the scope and been sampled, it averages each of the 2048 sets of three corresponding points to produce a waveform average and then signals the CPU that it is ready to send the average down. The CPU, when notified, signals the scope that it is ready to receive the waveform. The waveform is then sent and stored on the CPU's hard drive for future processing. The CPU now directs the pedestal to rotate to the next azimuthal setting, and the cycle repeats. Collecting data for all angle settings over the entire azimuthal range takes 30 min.
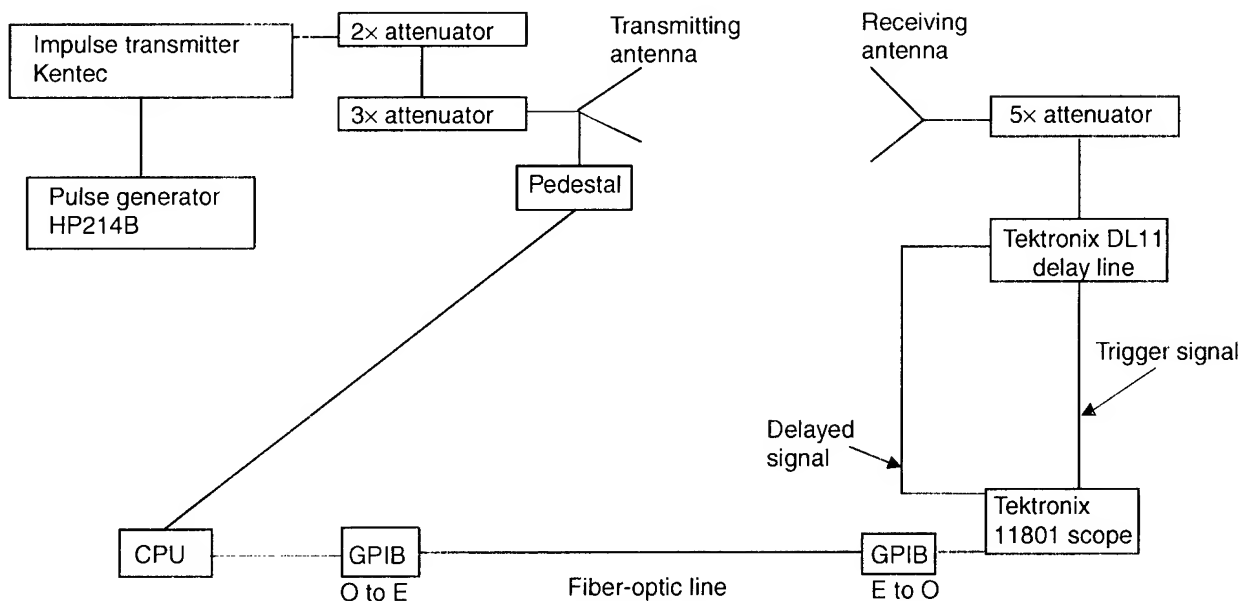

Figure 3. Electrical configuration of experiment in EMRF.

2.2 FD Setup

We utilized the experimental setup in the chamber to collect data in the FD, as opposed to the TD previously described. This setup is depicted in figure 4. The transmitting antenna is connected to port 1 of the HP8510c Vector Network Analyzer (VNA), and the receiving antenna is connected to port 2. The CPU controls the rotation of the pedestal as in section 2.1, except that the angle increment here is 2.5°. For each azimuthal setting, the VNA feeds 801 frequencies into the transmitting antenna. The frequencies range from 50 MHz to 10 GHz. At each frequency, 200 measurements of the power gain are taken and averaged. The entire set of measurements from –90° to +90° takes 240 min. The power gain of interest here is the ratio, expressed in decibels, of the power received to the power fed into the transmitting antenna. Averaging in the FD, as in the TD, cancels out as much noise as possible, i.e., enhances the signal-to-noise ratio (SNR). The results are shown in figures 5 and 6, which show gain versus frequency plots and gain versus azimuthal angle and frequency plots.

The chamber also served as a test environment for the UWB-UWA antenna evaluations. It is $50 \times 25 \times 30$ ft. It has an rf absorber attached to its walls that reduces the power of the reflected signals by at least 20 dB in the frequency range of 2 to 18 GHz (and ~10 dB below 1 GHz). Since this chamber is 50 ft long, any frequency components of a signal below 200 MHz are in the near field; i.e., those frequencies picked up at the receiving antenna may not provide meaningful far-field radiation information. The VNA is used in the FD measurements in the chamber. It was also configured in its time-gating mode to eliminate the calculated reflections from the chamber walls.

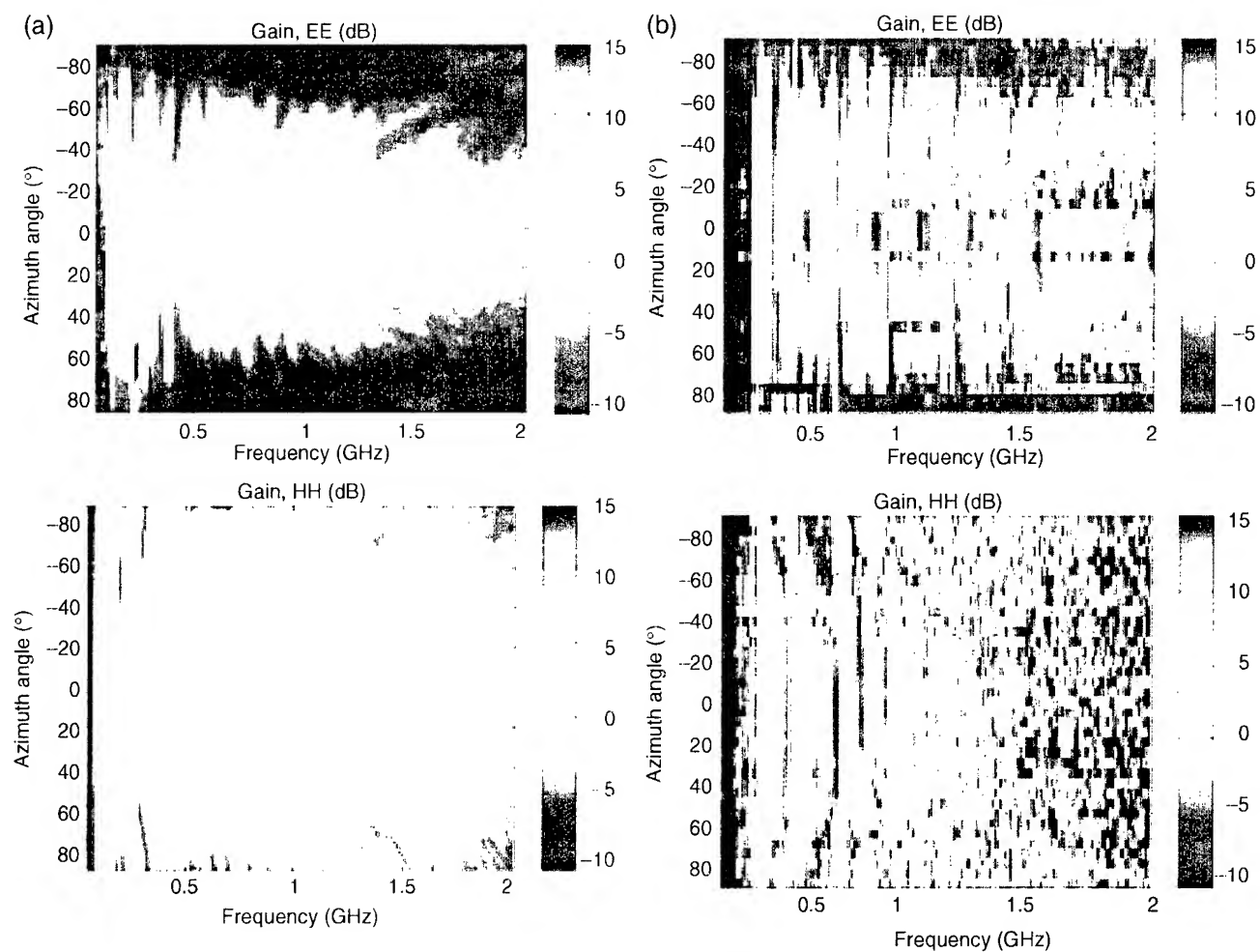Figure 4. Antenna configuration in Anechoic Chamber.
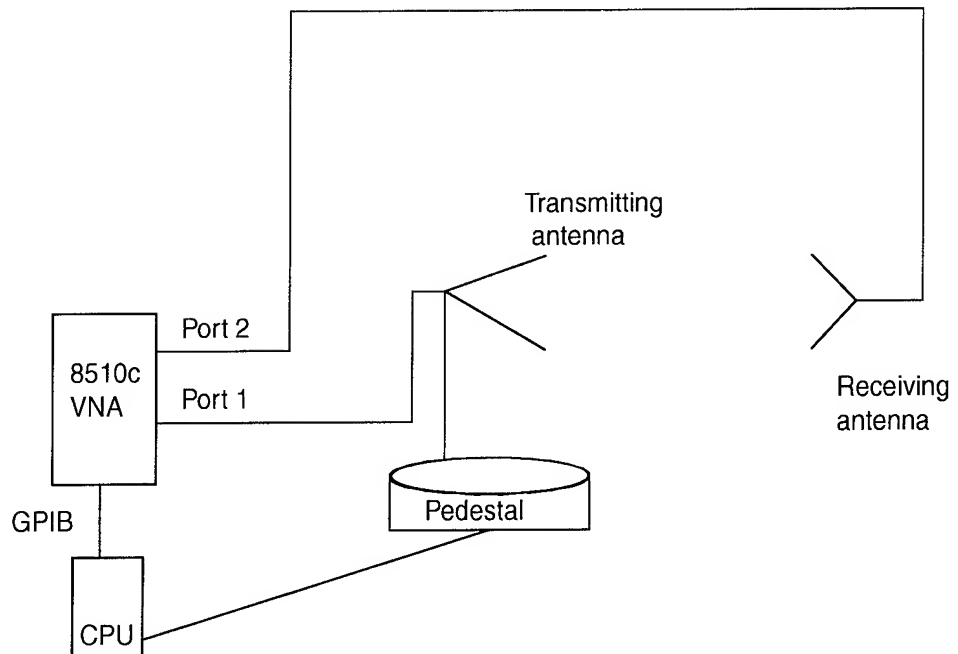
Figure 5. Commercial LP antenna radiation patterns measured with HP8510c VNA. Comparing results of (a) FD measurements and (b) TD measurements provides confidence of reproducible findings. EE and HH denote antennas were set to transmit and receive same orientation E-field and H-field, respectively.
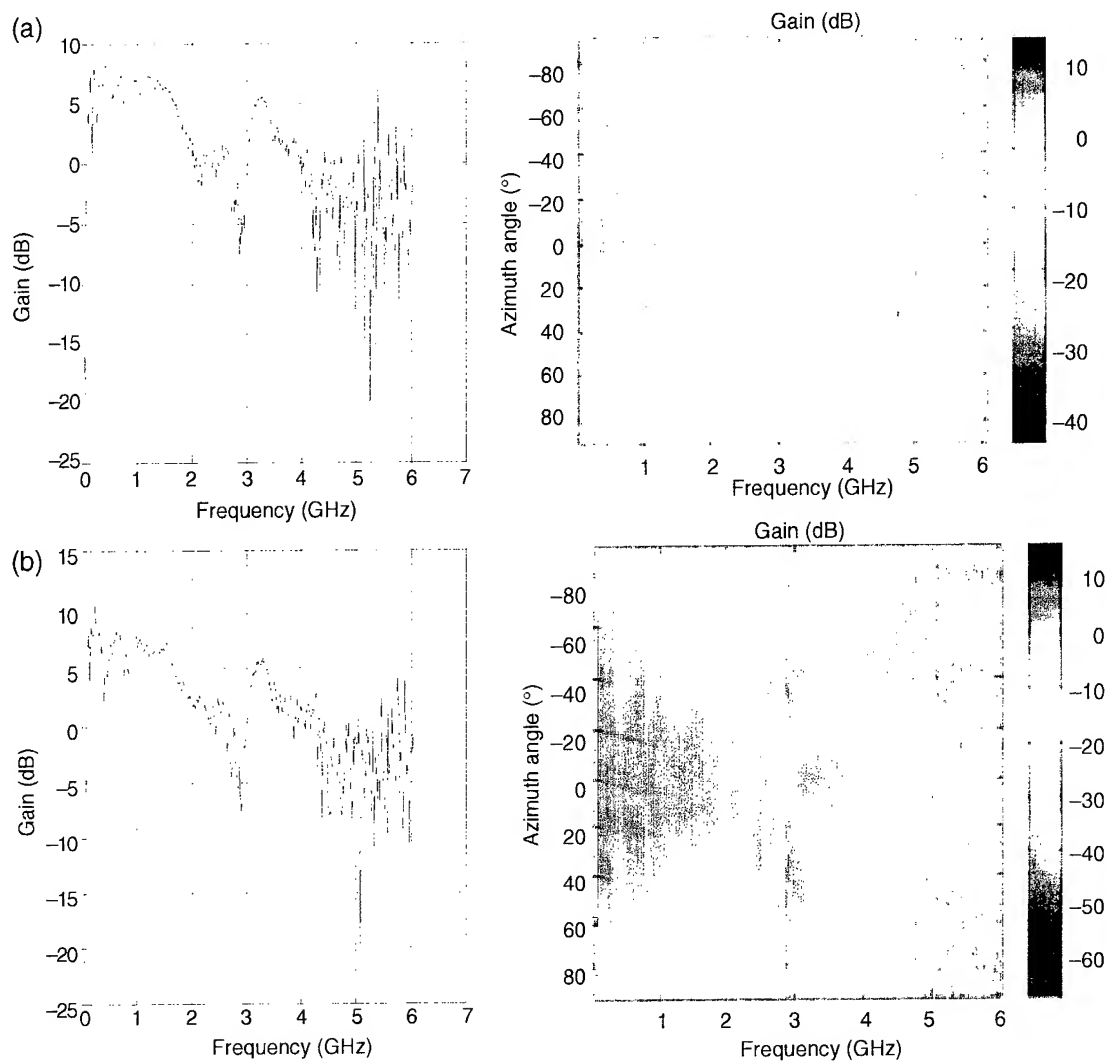
Figure 6. Comparison of (a) HH and (b) EE in FD. Left-hand plots are at azimuth angle of 0° and right-hand plots cover full azimuthal range.

2.3 Antennas

The three photographs in figure 7 show the UWB-UWA antenna close-up. It consists of two LP antennas that are perpendicular to each other and that are interlocking. Each antenna consists of a sequence of side-by-side parallel linear dipoles that form a coplanar array. The tapered envelope shown in figure 7(a) reflects the fact that the length of the individual dipoles in this array increases logarithmically as you travel down the center of the antenna. A crisscross connection links the dipoles. The inductive loading shown in figure 7(b) allows the antenna to radiate and receive longer wavelengths than its physical length by itself would permit. The dual polarization shown in figure 7(c) permits cross-polarization experiments to be performed.
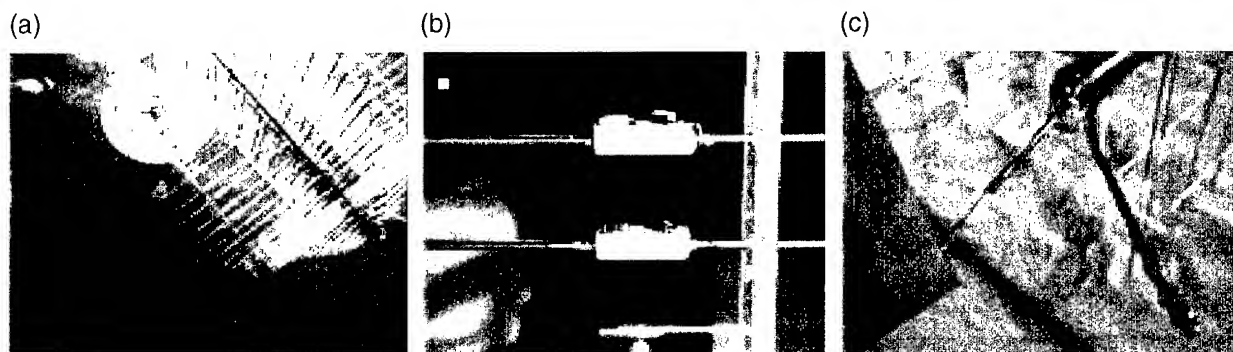
Figure 7. UWB-UWA LP antenna showing (a) tapered envelope, (b) inductive loading, and (c) dual polarization feeds.

The following is a note about the crisscross connection between the dipoles: Mechanically crisscrossing or transposing the feed between adjacent elements causes a phase angle of 180° to be added to the terminal of each element. Since the phase between the adjacent closely spaced short elements is almost in opposition, they radiate very little energy, and their interference effects cancel out. At the same time, the longer and more widely spaced elements do radiate. The mechanical phase reversal between these elements produces a phase progression so that the energy is beamed in the direction of the shorter elements. The most active elements of this feed arrangement are those that are nearly resonant, and their combined radiation pattern lies toward the vertex of the end-fire array.

2.4 Kentec Impulse Source

The frequency content of the voltage output of the Kentec impulse source is shown in figure 8. The Matrix Laboratory (MATLAB) program "jtfa_axis_length.m" generated this plot and the one in figure 9. In figure 8, we see the fast Fourier Transform (FFT) of the output pulse on the left and its spectrogram on the right. The original shape of the pulse is evident in the figure 8 spectrogram. The subplot in the upper left-hand corner has a vertical axis representing frequency in hertz and a horizontal axis for energy in joules/hertz. The lower right-hand subplot has a vertical axis representing volts and simply depicts the original waveform. It starts a little after 2 ns, rises to a peak in ~150 ps, and then exponentially tapers off. Let us compare that with a plot of a pulse that was emitted from a UWB-UWA antenna. Figure 9 is the spectrogram of such a spread-out pulse. As can be seen from the colored intensity subplot, the radiated electric field from the UWB-UWA antenna takes the form of a frequency chirp. It extends in frequency up to 4 GHz, an observation consistent with the FFT in figure 10. What this spectrogram illustrates so vividly in figure 9 is that the original 3 ns pulses have been spread out to over ~75 ns. The dispersive design of an LP structure is responsible for the elongated output.

9

Figure 8. Kentec
impulse (horizontal plot
in TD), FFT (vertical
plot in FD), and joint
time-frequency plot
(spectrogram).
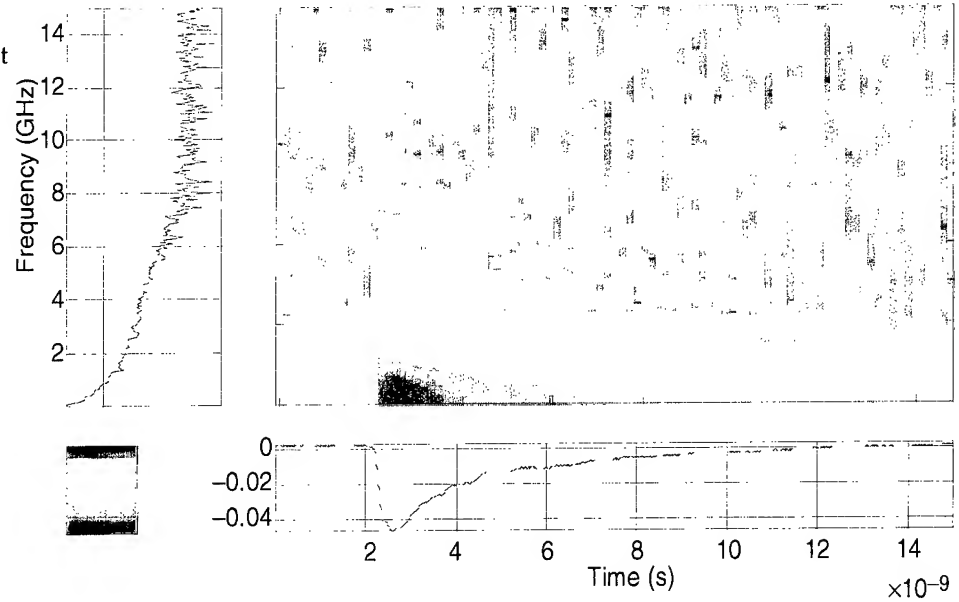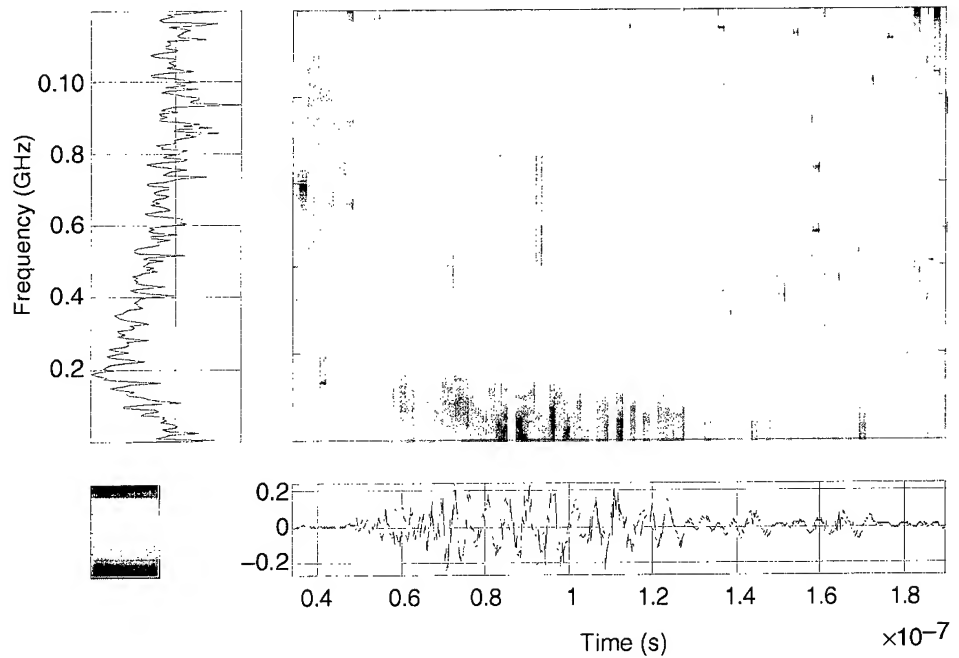
Figure 9. Spectrogram
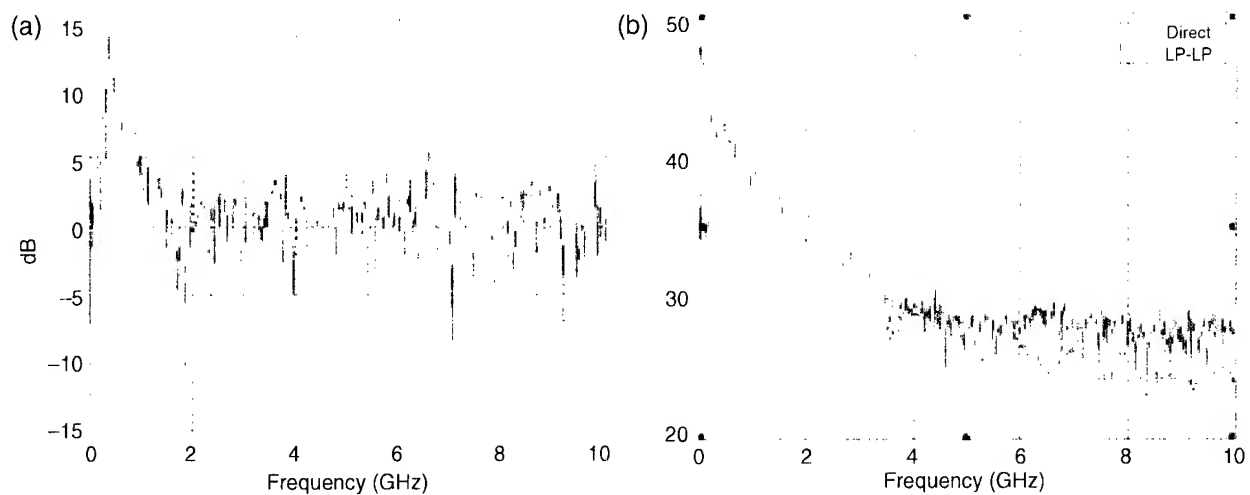of UWB-UWA pulse
after its emission from
UWB-UWA antenna.

10

Figure 10. (a) FFT of signal average of 3 waveforms and (b) FFT of signal average of 3000 waveforms and Fourier transform of original Kentec output pulse. Ambient noise floor is significant above 2 GHz. Signal averaging lowers noise floor, provides smoother response, and moves high-frequency limit up to 4 GHz.

3. Experimental Results

Over a period of two days, many waveforms were recorded. The convention among the figures that will be discussed is that those showing TD plots are based on measurements taken in the cathedral while those showing FD plots are based on measurements taken in the chamber. Data were acquired in both the E-plane and the H-plane. These modes correspond to the principal planes of the antenna, where for example, in the E-plane, the electric field of the antenna is in the plane of rotation of the pedestal. In each plane, the antenna pairs were also measured in copolarized and cross-polarized orientations.

The UWB-UWA antenna under test contains two cross-polarized LP antennas (UWB-UWA 1 and UWB-UWA 2) in the same cube package. Each was evaluated separately, and the data from each are labeled EE1 for the copolarized E-plane of antenna 1 and EE2 for the copolarized E-plane of antenna 2 (see figs. 11 and 12; see, specifically, fig. 11(c) and fig. 12(c)). The data from these new inductively loaded antennas are compared to radiation patterns of the commercially available LP antenna labeled LPEE for the copolarized E-plane and labeled LPHH for the copolarized H-plane, respectively (see fig. 13). All measurements on the UWB-UWA LP and the commercial LP used the commercial LP as the receiving component in the configuration.

Figure 11. TD waveforms for UWB-UWA inductively loaded LP antenna 1: (a) H-plane transmit, H-plane receive (HH1) (copolarized); (b) H-plane transmit, E-plane receive (HE1) (cross-polarized); (c) E-plane transmit, E-plane receive (EE1) (copolarized), and (d) E-plane transmit, H-plane receive (EH1) (cross-polarized).
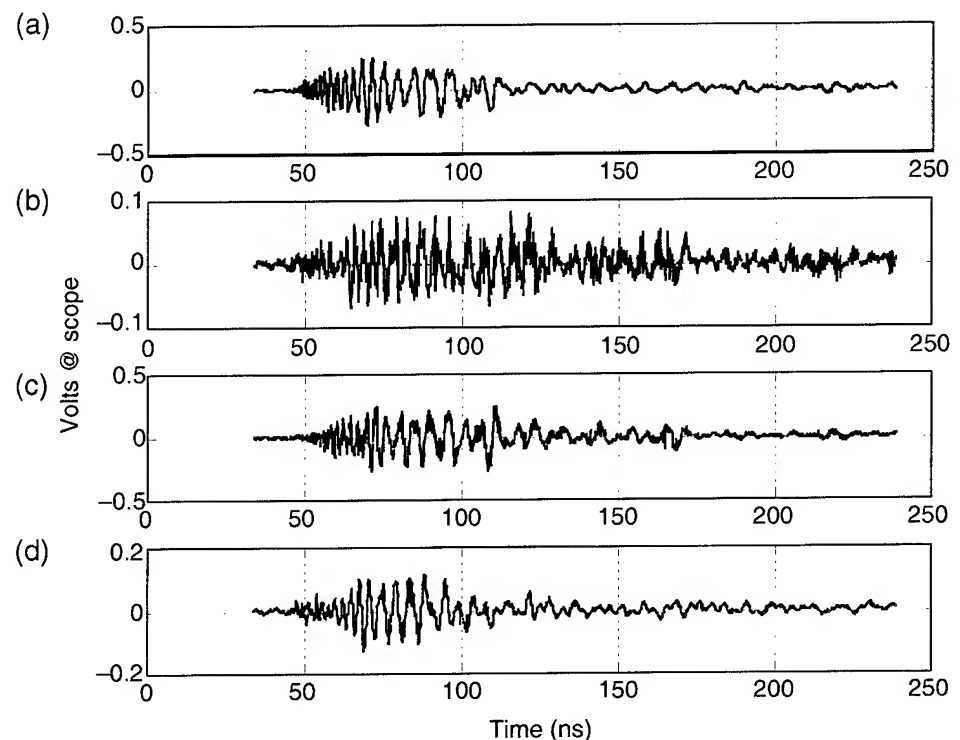
Figure 12. TD
waveforms for UWB-
UWA inductively
loaded LP antenna 2: (a)
HH2, (b) HE2, (c) EE2,
and (d) EH2.
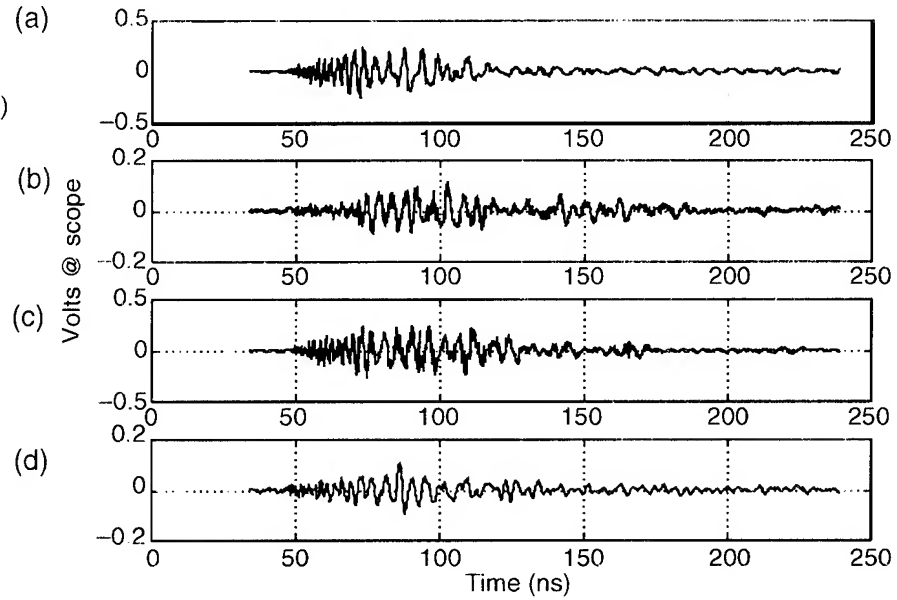
Figure 13. TD boresight
waveforms of
commercial LP antenna:
(a) LPHH4, (b) LPHE4,
(c) LPEE1, and
(d) LPEH1
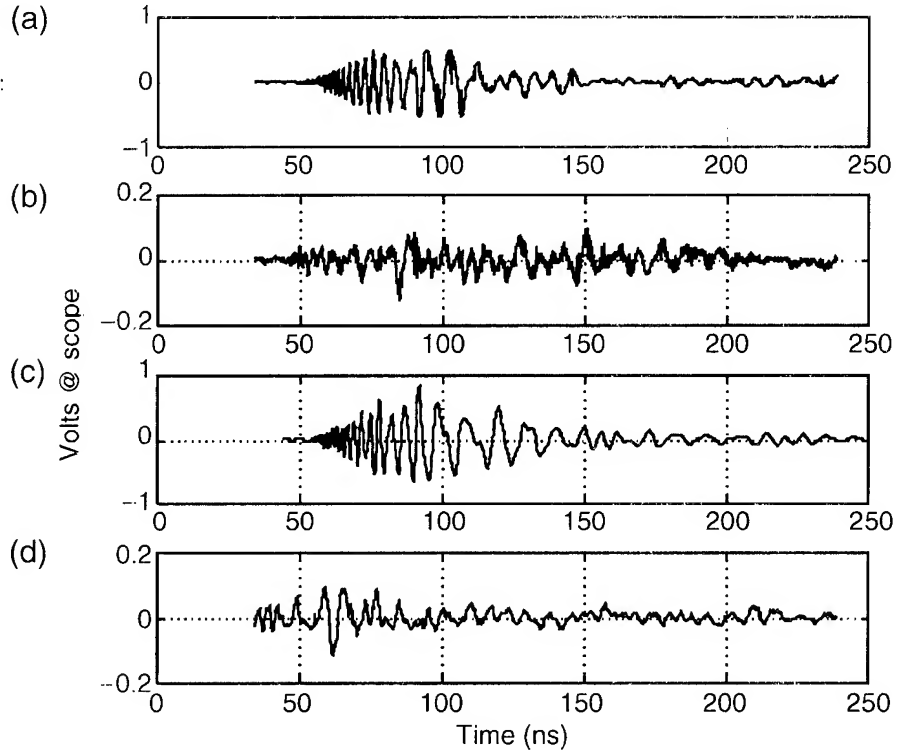
In summary, we evaluated three antennas: the commercial LP and both units of the inductively loaded UWB-UWA LP. Each antenna was measured with TD techniques. In addition, the commercially available LP was measured with the FD techniques, and the results were compared directly with those in the TD. With each technique and for each antenna, a radiation pattern was generated for both the copolarized and the cross-polarized configurations. Results are discussed in the next section.

13

3.1 TD Boresight Waveforms

A 1.9-kV impulse was fed into the UWB-UWA transmitting antenna. At the receiving antenna, a 12.5-V/m electric field was measured. After the impulse passed through this antenna and the delay line, an amplitude of 250 mV was measured on the sampling scope.

Figure 11 shows the basic copolarized and cross-polarized waveforms for the UWB-UWA LP. The antennas were copolarized if they were both set to transmit and receive the same orientation E-field or H-field. This is indicated by "HH" and "EE" in the caption. The cross-polarized plots represent a situation in which the transmitting antenna transmitted one field and the receiving antenna was polarized at 90° to that field. Cross polarization is indicated by "HE" and "EH" in the caption. The first letter in these designations refers to the polarization of the transmitting antenna, and the second letter refers to the polarization of the receiving antenna. For example, a designation of "HE" indicates the transmitting antenna is polarized in the H-plane while the receiving antenna is polarized in the E-plane. These plots show that the signal strength measured at the receiving antenna in the cross-polarized mode is 1/2 of that measured in a copolarized mode. This corresponds to a 10-dB cross-polarization isolation.

Figure 13 represents the results from a configuration in which the antennas are pointing directly at each other, boresight to boresight. The four plots were taken with two identical commercial LP antennas. Multipath reflections were superimposed on the original signal. Reflections off the sandbox lagged the start of the signal by ~22 ns and reflections off the garage door lagged by ~70 ns.

Figure 12 shows the waveforms recorded by the Tektronix 11801 for both polarizations of the UWB-UWA LP antennas. This figure shows the raw data taken on boresight for antenna 2 of the inductively loaded LP. These results are almost identical to the waveforms of antenna 1 (see fig. 11) colocated in the cube (see fig. 1(a)).

Figure 10 illustrates how increasing the number of waveforms underlying an average reduces the noise level. The plot on the left is an FFT of a signal average of three waveforms. Plainly, the ambient noise floor becomes significant above 2 GHz. This plot is in contrast to the plot on the right that shows the Fourier transform of a signal averaged with 3000 waveforms and the Fourier transform of the original Kentec output pulse (blue). The received signal average appears in green. In this plot, the noise floor is significant above 4 GHz. Hence, increasing the number of signals underlying an average reduces ambient noise and permits us to observe higher frequency components in the signal.

3.2 TD Radiation Patterns

In figure 14, the E-plane patterns (top row) and the H-plane patterns (bottom row) are compared for all three antennas, UWB-UWA 1, column (a); UWB-UWA 2, column (b); and commercial LP, column (c), respectively. The radiation pattern for the H-plane is spread out over the full azimuthal range of $-90°$ to $+90°$, whereas the E-field lies in a narrower angular band of $\sim -60°$ to $+60°$. The commercial LP antenna pattern reaches a maximum gain of 15 dB while the pattern for the other two inductively loaded UWB-UWA antennas reaches a maximum of only 10 dB. The trade-off of gain versus compact packaging and size should be expected. Also, the gain in the H-plane is present down to 150 MHz for the commercial LP antenna while the gain of the UWB-UWA antennas is present down to 300 MHz.

In general, the H-plane gain is about 10 dB greater than that of the E-plane gain (not shown are plots of boresight gain). The HH gain pattern extends out through the full azimuthal range, whereas the EE gain pattern falls sharply at an azimuthal angle over 60°. The cross-polarized patterns for UWB-UWA 1 exhibit a much lower gain than do the copolarized patterns, as would be expected (figures not shown.) The EH gain pattern is about 10 dB down from either of the copolarized patterns. The HE gain pattern is 15 to 20 dB down. The results for the UWB-UWA 2 are very similar to those for the UWB-UWA 1 and therefore are not repeated here.
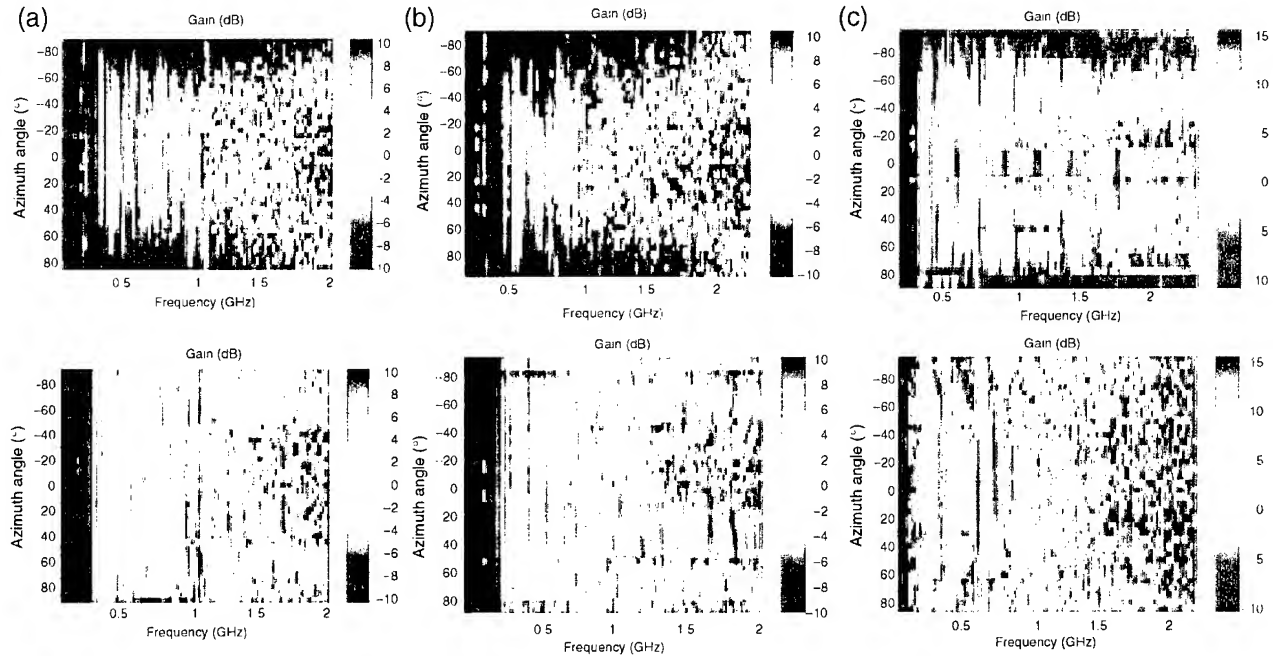

Figure 14. Radiation patterns for two copackaged, inductively loaded UWB-UWA antennas and commercial LP. Top row shows radiation pattern in E-plane of each antenna while bottom row shows H-plane radiation patterns. Patterns are generated by (a) UWB-UWA 1, (b) UWB-UWA 2, and (c) commercial LP antennas.

3.3 Comparison of FD and TD Measurement Results

In figure 5, the two radiation patterns on the left are based on FD data taken by the HP8510c VNA in the chamber, whereas the two radiation patterns on the right are based on TD data of the transmitted Kentec pulse that has been sampled by the scope in the cathedral and then processed by an FFT routine. The plots on the left were generated by having the 8510c step through and feed 801 frequencies between 50 MHz and 10 GHz to the UWB-UWA transmitting antenna and recording the response of the system at each frequency. The plots in both TD and FD show that the H-field has a broader pattern than the E-field over the full azimuthal range. We see that the E-field radiation pattern is primarily confined to between –60° and +60°, whereas the H-plane radiation pattern extends to 90° in both directions, as observed in TD. The H-plane frequency content measured in TD (on the right in fig. 5) extends to a lower frequency than that measured in the E-plane, a phenomenon not observed in FD data (on the left).

The right-hand plots (TD) in figure 5 have less low-frequency information than the left-hand plots because they exhibit only frequency components in the original Kentec pulse, whereas left-hand plots were the product of a VNA generating signals starting at 50 MHz. Perhaps the most important factor in comparing the two techniques is the presence of background noise in the open environment of the cathedral. The H-plane radiation pattern on the right is grainy, indicating more background noise. The E-plane pattern is also grainy, but not as much as the H-plane radiation. This could be overcome in the future by raising the voltage output level greater than the 1.9-kV voltage applied. The practical upper limits that can be used depend on the antenna under test and the environmental assessment limits under which we are legally constrained to operate.

Because of ambient noise shown in figure 10, we determined that the antenna patterns contained valid data only up to 2 GHz. We compared the commercial LP antenna in both principal planes (H-plane and E-plane) using both TD and FD techniques as described previously. The experimental setup in this case has both the transmitting and receiving antennas being the commercial antenna. The FD boresight gain (not shown directly), which corresponds to a 0° angle in the antenna patterns of figure 5, show that in both principal planes, the gain falls off at ~1.6 GHz.

In doing this comparison, we performed the same calibrations and characterizations on a pair of the commercial LP antennas. The EE boresight gain is predominantly at a level of 10 dB, with dropouts at 400 and 800 MHz (see fig. 5). It drops off below 100 MHz. The azimuth ranges from –60° to +60°. The HH radiation power gain also is fairly flat and extends to a lower frequency than EE before it drops. This result is true of both the UWB-UWA antennas—the H-plane pattern extends over the full azimuthal range. The radiation pattern plot is much noisier in the H-plane than in the E-plane. It is not clear why this should be so, but it could be because of a higher background noise environment when we took this data. One way to test this hypothesis is to take the same set of data at night when environmental noise is reduced.

The gain plots for the cross-polarized setup show that the gain is 15 to 20 dB below its level in the EE and HH setups. The EH radiation pattern is weighted toward the low end of the 0 to 2 GHz range while the HE pattern is weighted toward the upper end. Again, it is not clear why this should be so. Further investigation is necessary to understand this result and to determine if it is reproducible at night when there is less background noise.

3.4 High-Voltage Limit of UWB-UWA Antenna

In the chamber, we ran a test to determine how high of a voltage the UWB-UWA antenna could handle and still function properly. When the antenna was fed a 7500-V signal, it functioned properly. When the antenna was fed a 15-kV signal, corona was discharged at the antenna feed. This discharge blocked EM transmission from the antenna. We performed this stress test after taking all radiation measurements. This antenna was checked after the stress test to determine if it suffered damage and was found to still be operational.

3.5 Noise Reduction

If we compare the EE and HH gain plots for the commercial LP antenna in figure 6 with those plots in figures 15 and 16, we observe that the gain plots in figure 6 exhibit little noise, whereas those plots in figures 15 and 16 exhibit a high-noise level. Figure 5 exhibits the same phenomenon but in a different manner. The plots on the left are much smoother than their counterparts on the right, which are grainy, especially the lower one. This graininess is symptomatic of a high noise level. We also saw in figure 10 how increasing the number of waveforms in signal averaging reduces noise. There, the frequency components of the signal, which diminish in amplitude as the frequency increases, were not obscured by noise until 4 GHz was reached.

What accounted for the reduced noise in all these plots was increasing the number of waveforms underlying an average. In the TD for each average, there were three waveforms, each consisting of 2048 points, so that 6144 data points were recorded at each angle. By contrast, the FD plots had 801 frequency points, with each point being the average of 200 readings, so that 160,200 data points were recorded at each angle. This noise reduction can be explained by a statistical theorem that states that if a random variable is derived by taking the mean of n independent random variables, each with the same mean and standard deviation (σ), then the derived random variable has a standard deviation that is $\sigma/\sqrt{n}$. Furthermore, if each of the random variables can be described by a Gaussian distribution, which is the case here, than 2/3 of the variable values fall within 1 standard deviation of the mean, 95 percent fall within 2 standard deviations, and 99 percent fall within 3 standard deviations. This means that as you increase the number of measurements that underlie the mean of a random variable, then the variability of that mean is going to diminish. Less variability over the range of the plot translates into a smoother plot with less graininess.
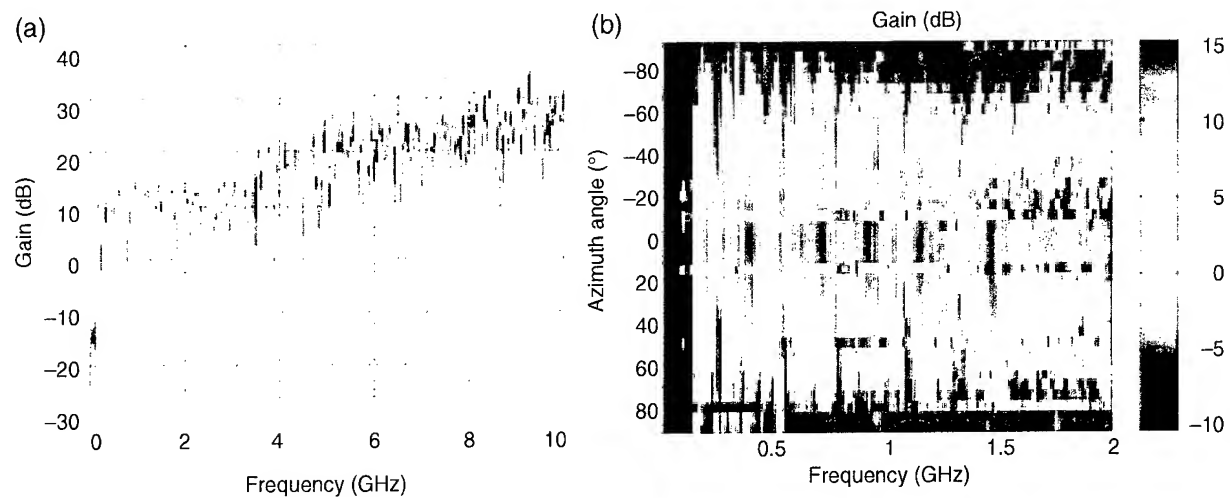
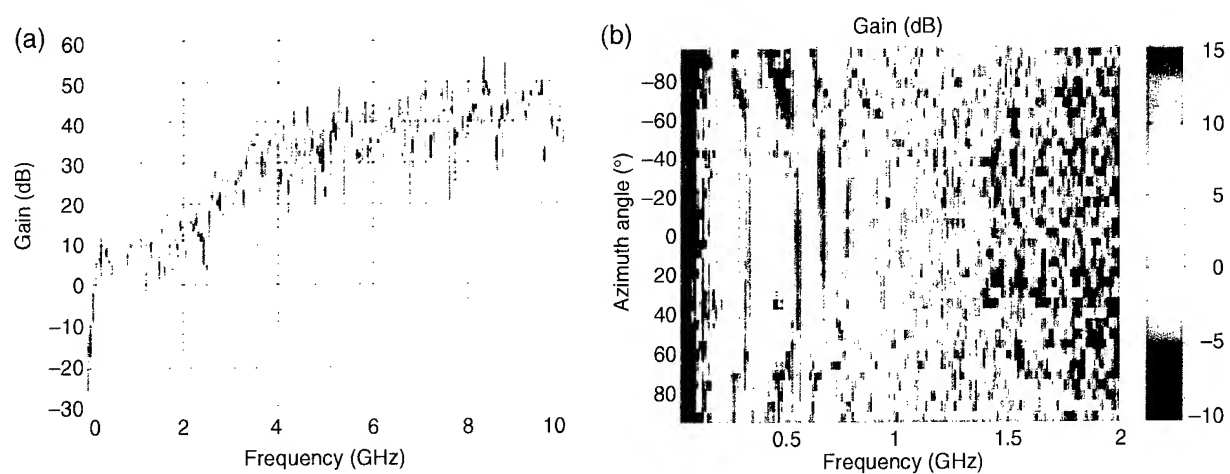Figure 15. LP EE radiation pattern (a) at azimuth angle of 0° and (b) for full azimuthal range.

Figure 16. LP HH radiation pattern (a) at azimuth angle of 0° and (b) for full azimuthal range.

18

4. Conclusions

The UWB-UWA 1 and UWB-UWA 2 antennas had similar radiation patterns for various combinations of the *E*- and *H*-planes in transmitting and receiving modes. For all three antennas, the *H*-plane radiation covered the full azimuthal range while *E*-plane radiation was spread out approximately from −60° to +60°.

We saw that the SNR in the FD was much higher than in the TD. In the FD, 160,200 data points (801 points × 200 measurements) were taken at each angle setting, whereas in the TD, 6144 points (3 waveforms × 2048 points) were taken at each angle setting. Taking the time to collect additional data points benefited in smoother radiation pattern plots in the FD as compared to the TD. This smoothness was the consequence of eliminating much of the noise. It also shows that the FD plots represent more information than the TD plots. The fact that increasing the number of waveforms going into an average reduces noise was strikingly illustrated when a gain plot based on 3000 waveforms was compared with one based on just 3 waveforms. All frequency components above 2 GHz were swamped by noise in the plot based on 3 waveforms while frequency components up to 4 GHz were clearly visible in the plot based on 3000 waveforms.

The collection of 160,200 data points at each angle setting for FD plots took 240 min. for the entire range of −90° to +90°. The collection of 6144 data points at each angle setting for TD plots took 30 min. for the entire azimuthal range. This would suggest that collecting FD data is 3 times more efficient than collecting TD data. If we consider that the azimuth settings in the chamber were 2.5° apart, whereas those in the cathedral were 5° apart, then FD collection is 6 times more efficient than TD collection. If we want to apply in the future what we learned about noise reduction, then the same experiment can be performed in the cathedral as before, except that instead of averaging with 3 waveforms, we would average with 3000. Some problems with this approach would be greatly increased measurement times and wearing out of the Kentec impulse transmitter under the stress of such prolonged use.

Another possible refinement would be to apply time-gating. Time-gating would greatly reduce the contamination of the received signal from multipath reflections. In the cathedral, the first multipath reflection arrived 22 ns after the beginning of the signal, so time-gating might be applied 25 ns after the signal begins.

The cathedral environment offers a large volume that greatly eliminates the effects of reflection and scattering; however, in the relatively open EM environment that the cathedral provides, we find an ambient noise background of radio, communications, and radars of the Baltimore-Washington area that reduces the sensitivity with which we can measure the calibration signals of interest.

19

Distribution

Admnstr
Defns Techl Info Ctr
Attn DTIC-OCP
8725 John J Kingman Rd Ste 0944
FT Belvoir VA 22060-6218

Ofc of the Secy of Defns
Attn ODDRE (R&AT)
The Pentagon
Washington DC 20301-3080

Ofc of the Secy of Defns
Attn OUSD(A&T)/ODDR&E(R) R J Trew
3080 Defense Pentagon
Washington DC 20301-7100

AMCOM MRDEC
Attn AMSMI-RD W C McCorkle
Redstone Arsenal AL 35898-5240

Dir for MANPRINT
Ofc of the Deputy Chief of Staff for Prsnnl
Attn J Hiller
The Pentagon Rm 2C733
Washington DC 20301-0300

SMC/CZA
2435 Vela Way Ste 1613
El Segundo CA 90245-5500

TECOM
Attn AMSTE-CL
Aberdeen Proving Ground MD 21005-5057

US Army ARDEC
Attn AMSTA-AR-TD M Fisette
Bldg 1
Picatinny Arsenal NJ 07806-5000

US Army Info Sys Engrg Cmnd
Attn AMSEL-IE-TD F Jenia
FT Huachuca AZ 85613-5300

US Army Natick RDEC Acting Techl Dir
Attn SBCN-T P Brandler
Natick MA 01760-5002

US Army Simulation, Train, & Instrmntn
    Cmnd
Attn AMSTI-CG M Macedonia
Attn J Stahl
12350 Research Parkway
Orlando FL 32826-3726

US Army Soldier & Biol Chem Cmnd Dir of
    Rsrch & Techlgy Dirctrt
Attn SMCCR-RS I G Resnick
Aberdeen Proving Ground MD 21010-5423

US Army Tank-Automtv Cmnd RDEC
Attn AMSTA-TR J Chapin
Warren MI 48397-5000

US Army Train & Doctrine Cmnd Battle Lab
    Integration & Techl Dirctrt
Attn ATCD-B
FT Monroe VA 23651-5850

US Military Academy
Mathematical Sci Ctr of Excellence
Attn MDN-A LTC M D Phillips
Dept of Mathematical Sci Thayer Hall
West Point NY 10996-1786

Nav Surfc Warfare Ctr
Attn Code B07 J Pennella
17320 Dahlgren Rd
Bldg 1470 Rm 1101
Dahlgren VA 22448-5100

DARPA
Attn S Welby
3701 N Fairfax Dr
Arlington VA 22203-1714

Distribution (cont'd)

Hicks & Associates Inc
Attn G Singley III
1710 Goodrich Dr Ste 1300
McLean VA 22102

Mission Rsrch Corp
Attn G Salo
3975 Research Blvd
Dayton OH 45430-2108

Palisades Inst for Rsrch Svc Inc
Attn E Carr
1745 Jefferson Davis Hwy Ste 500
Arlington VA 22202-3402

Director
US Army Rsrch Ofc
Attn AMSRL-RO-D JCI Chang
Attn AMSRL-RO-EN W D Bach
PO Box 12211
Research Triangle Park NC 27709

US Army Rsrch Lab
Attn AMSRL-CI-AI-R Mail & Records Mgmt
Attn AMSRL-CI-AP Techl Pub (3 copies)
Attn AMSRL-CI-LL Techl Lib (3 copies)
Attn AMSRL-DD J M Miller
Attn AMSRL-SE-DP L Cheskis
Attn AMSRL-SE-DP L Dilks
Attn AMSRL-SE-DP M Litz (20 copies)
Attn AMSRL-SE-DP N Tesny
Attn AMSRL-SE-DP R A Kehs
Attn AMSRL-SE-EO D Smith
Attn AMSRL-SE-RU M Ressler
Adelphi MD 20783-1197

REPORT DOCUMENTATION PAGE

1. AGENCY USE ONLY *(Leave blank)*	2. REPORT DATE February 2001	3. REPORT TYPE AND DATES COVERED Final, 11/99

4. TITLE AND SUBTITLE Characteristics of an Ultra-Wide-Band Ultra-Wide-Angle Log-Periodic Antenna

5. FUNDING NUMBERS

DA PR: —

PE: 62120A

6. AUTHOR(S) Leland M. Cheskis, Marc S. Litz, Neal Tesny, and Lillian Dilks

7. PERFORMING ORGANIZATION NAME(S) AND ADDRESS(ES)
U.S. Army Research Laboratory
Attn: AMSRL-SE-DP   email: lcheskis@arl.army.mil
2800 Powder Mill Road
Adelphi, MD 20783-1197

8. PERFORMING ORGANIZATION REPORT NUMBER
ARL-TR-2254

9. SPONSORING/MONITORING AGENCY NAME(S) AND ADDRESS(ES)
Mission Research Corporation
3975 Research Blvd
Dayton, OH 45430-2108

10. SPONSORING/MONITORING AGENCY REPORT NUMBER

11. SUPPLEMENTARY NOTES
ARL PR: 0NX3XX
AMS code: 622120.H16

12a. DISTRIBUTION/AVAILABILITY STATEMENT Approved for public release; distribution unlimited.

12b. DISTRIBUTION CODE

13. ABSTRACT *(Maximum 200 words)*
A compact ultra-wide-band, ultra-wide-angle log-periodic antenna has been designed by the Mission Research Corporation under a small business innovative research phase II contract with the U.S. Army Research Laboratory (ARL). A proof-of-principle version of the antenna was delivered to ARL. The antenna was evaluated within two days and information returned to the vendor. The calibrations of the antennas included both frequency-domain and time-domain measurements in the High-Power Microwave Anechoic Chamber and the Electromagnetic Research Facility, respectively, and high-voltage-limit characterizations. The appropriate conversion of time-domain and frequency-domain data into gain curves was performed, and the results were discussed. These results are now being applied to the next version of the dual-polarization antenna pair.

14. SUBJECT TERMS Copolarized, cross-polarized radiation pattern, time domain, frequency domain

15. NUMBER OF PAGES
28

16. PRICE CODE

17. SECURITY CLASSIFICATION OF REPORT Unclassified	18. SECURITY CLASSIFICATION OF THIS PAGE Unclassified	19. SECURITY CLASSIFICATION OF ABSTRACT Unclassified	20. LIMITATION OF ABSTRACT SAR